

Original Research

Application of Electrical Resistivity Tomography for the Assessment of Sinkhole Hazard to Improve Public Health and Safety Conditions on Post-Mining Lands

Rafał Jendruś^{1*}, Grzegorz Strozik¹, Dawid Sowiński²

¹Department of Mining, Safety Engineering and Industrial Automation, Silesian University of Technology, Gliwice, Poland

²Geosolum Company, Orłąt Lwowskich 122, 41-208 Sosnowiec/Poland

Received: 15 December 2022

Accepted: 19 April 2023

Abstract

In post-mining areas where hard coal mining took place under a thick overburden of carbonate rocks, there are often geomechanical threats occurring to the designed and existing buildings. They manifest by the occurrence of post-mining voids and deformations created in the Carboniferous layers and related to erosive processes, including karst ones occurring in the rock environment carbonate. Various geophysical research methods, including electrical resistivity imaging, find application in the assessment of deformations in the rock mass. Geophysical surveys may be applied to assess the necessity of carrying out treatment and protection works, e.g., borehole injection and determination of the boreholes' number and location. The paper presents two case studies of geophysical surveys using the method of two-level electrical resistivity profiling (ERP) and electrical resistivity tomography (ERT) in two adjacent research areas with a similar geological structure and a similar scope of mining operations. Based on the analysis of the obtained results, injection of voids and zones of a loosened ground in both areas was designed and executed. The analyzed cases have shown that methods of geophysical ground investigation based on electrical resistivity imaging provide accurate forecasting of the bedrock structure and can be used in practice to reliable determination of the threats to the ground surface from discontinuous deformations and their successful elimination.

The authors of this article performed the following research and their interpretation independently. They have appropriate geological and geophysical qualifications and many years of practical experience. The above allowed us to present in this article the issue, the need to select and the course of geoenvironmental procedures in areas where, on the one hand, shallow mining operations were

*e-mail: Rafal.Jendrus@polsl.pl

conducted, and on the other hand, the presence of complex geological conditions (karst phenomena) was found.

Keywords: post-mining areas, post-mining voids, Electrical Resistivity Tomography, injection of voids, public safety

Introduction

Discontinuous deformations of the earth's surface posing a threat to public safety occur most often as a result of karst phenomena [1], landslides [2] and underground mining [3, 4].

Underground coal mining worldwide is deteriorating the local mining environment in different ways. Ground subsidence, air pollution, vegetation pollution and water pollution have become important environmental threats caused by coal mining activities. Among them, environmental damage caused by ground subsidence is one of the problems to be solved [5].

The scale and intensity of subsidence represents a significant environmental impact. Soil is a critical component of the environment and represents the resource most impacted by the subsidence. Surface collapse for example, represents a catastrophic change in soil environment from which an area may not recover on a given time scale, [6].

The risk of discontinuous deformations on the surface of the area subjected to underground mining is directly related to the presence of large-size voids or strongly eroded zones of cracks and loosening in shallow layers of the ground, which may collapse in the event of loss of force balance in the ground.

Under the conditions of the hard coal deposit in the Upper Silesia Coal Basin (USCB), there are two main models of the geological structure of the layers in which discontinuous deformations may occur, [7]:

- The presence of Carboniferous layers with mined coal seams at a depth of up to a maximum of about 100 m, covered only with a thin overburden of loose Quaternary formations;
- The occurrence of the Triassic carbonate rock formation reaching the earth's surface lying on the Carboniferous more in-depth strata system, in which, apart from erosive and karst phenomena, there may be the effects of deep coal mining and shallow metal ore mining that favor the formation of discontinuous deformations;
- For a sinkhole to occur, the presence of underground voids, which can be [8, 9];
- The remnants of primary mining workings and secondary voids in the overburden of the mined deposits, resulting from the movement of rock masses from the surface to the primary voids (in post-mining areas);
- Voids, systems of fissures, fractures, and loosening occurring especially in rocks susceptible to erosion and suffosion phenomena (loose Quaternary formations and carbonate Triassic rocks).

The formation of discontinuous deformations related to underground mining activities can be generally ascribed to three types of mass movements in the rock mass, differing in their dynamics and course of the process [7, 10]:

- Collapse of large-size voids roof (resulting from erosive processes and mining activities) and the associated fall of roof rocks up to the ground surface (this is usually a dynamic and sudden phenomenon, as a result of which a sinkhole usually occurs);
- Clamping of loosened layers (formed systems of fractures or individual cracks) by overlying rocks, which are displaced vertically, leading to a lowering of the ground surface (in this case, the dynamics of the process is usually lower, and the effect may be a trough deformation);
- Filling with fine-grained granular material lifted from the overburden by migrating rainwater in the processes of suffosion and advection; the process may take place at a different pace and dynamics, from very slow (accompanied by the formation of depression basins) to rapid filling of large voids (runoff of a swamp causing the formation of a sinkhole).

Mechanical and chemical susceptibility, advective lifting, and other degradation processes of the rock medium combined with accumulation processes (clogging, sedimentation, crystallization) create a dynamic system of rock material movement in the rock mass, which results in deformation of the terrain surface and its subsoil, which may pose a threat to building structures on it. The effects of mining activities in the form of remains of mining workings, post-extraction voids, and rock mass deformation (cracks and subsidence) may intensify these processes in terms of quantity (frequency and number of occurrences in a given area) and qualitative (deformation size).

Propagation of the underground void towards the earth's surface and the duration of an uncollapsed void existence in the rock mass are practically independent of time. Ground deformations (sinkholes) may occur rapidly, and their time may be shifted in relation to the void formation by even several dozen years. A wide range of triggers may cause collapsing of underground voids, such as [11-13]:

- Deterioration of physical stability of the rock mass due to progress of karst processes;
- Changes in hydrogeological conditions;
- Changes in the structure of the rocks surrounding the void (impact of water migration or secondary fracturing);

- Reactivation of old and shallow cavings as a result of mining in greater depths („rejuvenation of inactive cavings);
- Rock mass shocks (paraseismic events resulted from rapid discharge of the potential energy of rock elasticity in the rock mass disturbed by mining activities);
- Climate and meteorological phenomena - intensive rainfalls, alternating between freezing water and melting ice;
- Anthropogenic factors, i.e. - tree felling, changes in the stress distribution in the ground by civil engineering and construction works, vibrations generated by machines and vehicles and other.

Karst processes

Karst processes are a type of chemical erosion, found in carbonate rocks such as limestone [14, 15] and dolomite [16]. They rely on the dissolution of calcium carbonate by water with the participation of carbon dioxide (carbonate karst), halite and sylvite (salt karst), gypsum and anhydrite (gypsum karst) - the latter two types of karst do not require the presence of carbon dioxide to dissolve minerals in the water. As a result of the solution's drying, reverse reactions occur, leading to the formation of various karst formations and forms (the so-called positive karst). Karst phenomena are a frequent cause of discontinuous surface deformations. They occur when carbonate strata lying at a shallow depth are covered with easily permeable sediments of young (Quaternary) deposits. Rainwater infiltrates limestone massifs (dolomites, marls, gypsums, and others) through natural fissures and cracks, causing their gradual widening, favoring the increase in the speed of movement of these waters in the cracks and intensification of the carbonate rock karst process. As a result, in more prone to dissolution formations, karstic troughs, voids, and caverns are formed, which can become quite large. This mechanism is responsible for the formation of karst caves. Karst processes can result

in large-scale voids - extensive fissures and caverns - and can lead to the creation of spongy or porous rocks. The natural consequence of karst is that the voids are filled with a mixture of fine rock grains and rock fragments from loose layers of overburden, which in turn is manifested by the occurrence of sinkholes and other forms of discontinuous deformations on the surface of the land [17-19].

Therefore, the lithological description and petrographic analysis of geological parameters are essential for evaluating the physical and chemical characteristics that determine an aggregate's geoenvironmental behaviour [15].

One of the possible mechanisms for the development of karst phenomena leading to the occurrence of a sinkhole on the surface is shown in Fig. 1, [7]. Water from atmospheric precipitation passes through easily permeable layers of Quaternary sediments to fissured and cavernous carbonate layers, which cause the occurrence of slow suffosion phenomena in the overburden, with the gradual enlargement of gaps in the carbonate formations (Fig. 1a,b). With an excessive volume of karst voids, a rapid runoff of water along with the grains of loose rock formations may occur in the form of a quicksand runoff (Fig. 1c,d). In the case of the presence of cohesive layers over loose layers in the overburden, the surface deformation may in both cases be sudden, without warning symptoms in the form of shallow basins or small sinkholes.

The movement of water infiltrating the carbonate layers can be significantly intensified by drainage of underground mine workings (Fig. 1c,d).

A very important factor affecting the intensity of the erosion processes of the rock medium, the transport of sediments and their sedimentation is the free flow of groundwater. It depends on the geometry of fractures in compact rocks and the water permeability of loose rocks [15]. Due to the dynamics of flows in networks of voids and cracks, the water permeability of hard rocks is negligible.

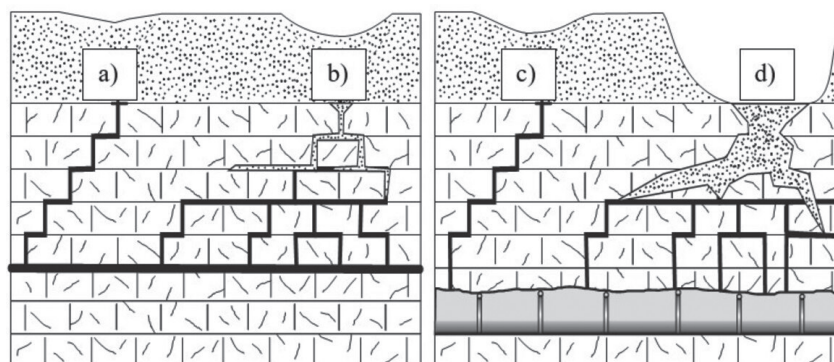


Fig. 1. Formation of discontinuous deformations as a result of karst phenomena: a) sinkhole formed as a result of rainwater infiltration into fractured layers with suffosive removal of soil particles, b) sinkhole formed as a result of rainwater infiltration with advective transport of soil particles into the developing fracture system, (c, d) intensification of deformation processes as a result of increased infiltration of groundwater into mining.

Voids within Carboniferous deposits in mine workings remnants and cavings (goaf zones) may create discontinuous deformations hazard. Loosened rock mass in favorable conditions negatively affects the Quaternary overburden's upper strata mainly through the suffosion process and uneven subsidence. In such a situation, the shallow grounds' physical and mechanical parameters, in particular non-cohesive soils, may undergo degradation.

The degradation mainly concerns the reduction of the degree of consolidation, and thus the deterioration of the degree of compaction indicating zones of loosened geological formations.

A particular risk of discontinuous deformations from post-extraction voids occurs when rocks and soil lying above the void may move to the void. This process can occur suddenly or slowly. The first case usually occurs when the insulating layer's continuity is broken between the void and the loose overburden and is typically associated with periodical severe waterlogging of the rock mass. Alternatively, the gradual lowering of the ground surface above the void, usually caused by suffosion, i.e., the transport of small particles of soil to the void, represents a slow process of surface discontinuities creation. As a result, a constant loss of soil mass in the overburden is advancing, which causes the ground surface to subside and crack. If the underground voids are sufficiently conductive and absorptive to transport significant masses of fine grains of soil and rocks from old, already filled with younger sediments sinkholes, they may be emptied again; such a process is referred to as reactivation of sinkholes.

In the aim to prevent deformation of the bedrock under the area designed for development, the rock mass injection or other ground stabilization works should be applied before the commencement of construction works. Their impact on the subsoil and bedrock is threefold:

- Filling the voids to prevent their collapse, clamping, and accumulation of transported erosion products and mechanical suffosion,
- Increase in strength parameters of weakened cracked and porous structures,
- Limiting the migration of groundwater and reducing the intensity of erosion processes in the formations exposed to them.

The effectiveness of injection treatments depends in no small extent on the choice of the number and location of boreholes, for which, in particular, a geophysical survey of the foundation of existing or planned building structures is predestined. This issue has been raised many times during the research [20-22], thanks to which many materials are confirming the legitimacy of using geophysical surveys for this purpose.

Geophysical research in the area of the risk of discontinuous deformations assessment may be performed for three purposes. In areas predisposed to the occurrence of discontinuous deformations, geophysical surveys should be applied before the commencement

of construction works in order to assess the risk of the occurrence of discontinuous deformations. In the case of existing deformation phenomena, the survey should be used to recognize their extent, the risk of their expansion and propagation, and the possibility of creating new ones. If there are voids, fracture networks, and relaxation zones in the subsoil that require active preventive measures, consisting, i.e., of filling them with injection mixtures, geophysical research results are used to optimize the location of injection wells. Finally, after completing of injection works, another verification test of the subsoil is performed to assess the effectiveness of the performed works in the area of liquidation of anomalous zones.

Due to the construction of shallow rock layers, the nature of the structures being the subject of the location and the scope of the test depth (up to about 100 m below the earth's surface), electrical resistivity imaging measurements are most often used, among which the most popular is ERT (Electrical Resistivity Tomography), [23-25]. Seismic methods are also frequently used, especially MASW (Multichannel Analysis of Surface Waves - in the active MASW 1D/2D/3D version and the passive MAM/ReMi 1D), [26, 27]. Their applicability is limited by the maximum depth, which for the active MASW 1D/2D/3D method ranges from 25 m to 40 m depending on the geological structure of the rock mass, and for the passive MAM/ReMi method from 50 m to 65 m [28, 1]. The microgravimetric method is less useful, giving good results rather than in the case of locating large-sized voids (mine workings) at a depth of up to about 50 m [29] and georadar (ground-penetrating radar GPR). In geophysical research related to the risk of deformation of the discontinuous terrain surface, GPR is useful for recognizing shallow discontinuities up to a depth of several meters, below which interpretation difficulties arise related to the differentiation of the structure of the rock mass, medium density, and water level [30, 31]. Nevertheless, since GPR research is quick and cheap to implement, it is often performed as a supplementary test to another method, such as ERT, to localize better the occurring anomalies and their nature [32].

In the face of a very wide range of available methods of geophysical research of the subsoil and practically unlimited variants of the geological structure of this subsoil, its hydrogeological and geomechanical properties, physical and meteorological phenomena occurring in a given location, the history of mining operations and many other conditions, the selection of an adequate method of geophysical research for a given case is not a trivial issue. To some extent, it is possible to approximately determine which methods of geophysical research may have good prognosis in given conditions, but the final confirmation can only be obtained with the use of sufficiently numerous and deep exploratory boreholes.

Material and Methods

The paper presents two case studies of the assessment of the risk of discontinuous deformations of the surface occurrence along with the location of boreholes for the injection works and the assessment of the quality of the forecasts based on the analysis of the volume of injected grout mixture, using the ERT method in two variants, in similar geological conditions. The obtained results allow to conclude about the usefulness of the ERT method for assessing the degree of risk of discontinuous deformations of the surface of the ground lying directly above the mass of carbonate rocks subjected to the influence of earlier hard coal mining operations in the deeper Carboniferous strata.

Geophysical recognition of the possibility of continuous and discontinuous deformations as well as the search for voids within the Triassic formations was carried out using the electroresistance profiling method in the medium gradient system.

The electro-resistance method is based on the variation of resistance between disturbances such as voids, caverns, fissure zones, etc., and the surrounding undisturbed rocks. The measuring system generates an artificial electric field in the ground and enables the measurement of its voltage on a specific section on the ground surface. The measurement results are the basis for calculating the apparent resistivity of the ground. The choice of the depth range (application of a specific measurement system) is conditioned by a specific, often complex geological and mining situation.

The depth range of the electrofusion method depends on the distance between the power electrodes driven into the ground (in geoelectrical methods marked as current electrodes A and B) as well as on the lithology of the given area. The potential difference between the

measuring electrodes is measured.

To carry out the task in question, in the field tests carried out on the measurement field, two measurement spacings $AB = 270$ m and $AB = 540$ m were used in a grid of measurement points every 5 meters. The first measurement spacing $AB = 270$ m reaches the depth range, which is estimated on the basis of many years of experimental work at approx. 65-70 m below ground level. The depth range of the spacing between the current electrodes $AB = 240$ m is estimated at approx. 125-135 m.

Geological Conditions

The areas A and B are undeveloped plots intended for industrial development. In terms of geology, the area under consideration is located within the Quaternary, Triassic, and lower Carboniferous formations boundary, Fig. 2. Clays and diluvial sands represent the Quaternary. When analyzing Poland's detailed geological map at the scale of 1: 50,000 - the Katowice sheet, diluvial sediments can be noticed at the western and eastern border of the A area and in the northern part of the B area. The diluvium has been created due to the erosion of the Triassic bedrock, material transport, and deposition. According to archival data, it is possible to note the occurrence of weathering with a thickness of more than 5 m. Based on the map and the measured heights, a strong correlation exists between diluvial deposits and the lowest area within the study's boundaries. This fact is confirmed by filling the eroded substrate with diluvial material coming from the higher Triassic strata. The Triassic formations, which belong to the Bytom Basin where both research areas are located, are represented by sediments of middle shell limestone and motley sandstone. The rock massif

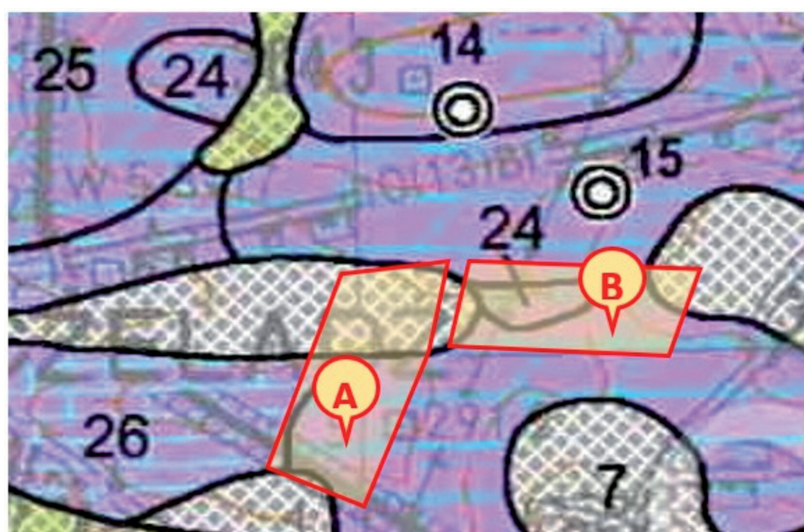


Fig. 2. Location of the research area on the geological map of Poland (original scale 1: 50,000, sheet 943 Katowice). 24 - Middle Triassic - Diplopora dolomite, 25 - Middle Triassic - ore dolomites, 26 - Middle Triassic - Gogolin strata, 7 - Quaternary - clays and deluvial sands, 14 - borehole (300.5 m; T2 - 0.0; T1 - 106.4 m; C3 - 125.6 (206.0 m); 15 - borehole (289.2 m; T2 - 0.0 m; T1 - 93.0 m; C3 - 110.0 m; (614.5 m); (T2 - Middle Triassic roof, T1 - Lower Triassic roof, C3 - Carboniferous roof).

takes the form of alternate strata of limestone, marl, and dolomites with clay contributions.

Based on the boreholes, the presence of Triassic formations in the form of limestone was demonstrated. Dolomites' occurrence was determined based on opencast zinc ore mines near the road from Będzin to Czeladź. When analyzing the archival materials, the presence of dolomite or dolomitic limestone in some parts of the studied area has been noted. Dolomite has also been documented as a layer below the limestone layer. The differentiation between the recorded rocks results from dolomite formation during the process of dolomitization of carbonate rocks. Due to the uneven course of the phenomenon mentioned above, some subsurface Triassic sediments were formed in limestone, dolomitic limestone, or dolomites.

The Carboniferous Formation lies below the Triassic bedrock. The roof of the Carbon formation lies at a depth of about 100 m - 140 m. It is developed as a series of mudstones and sandstones strata interlayered with numerous coal seams. The layers extend in the NW-SE direction and sloping down towards SW. Moreover, within the Carboniferous rocks, tectonic activity in the form of a network of faults is visible. Area A is crossed by the Northern fault of 100 m throw, which belongs to the regional tectonic structure, Figs 3 and 4.

The most important issue in the analyzed case was the selection of the appropriate method of geophysical research, along with the adopted depth range.

As it was mentioned earlier (in consultation with the Investor of the construction project in question), the overriding goal was to verify the presence of voids within the Triassic period.

On the basis of Fig. 2 (analysis of archival research wells - 14 and 15) and several research and appraisal wells made in the analyzed investment areas, it was confirmed that the Triassic formations formed in the form of limestones and dolomites. They are deposited to a depth of 60 m below ground level, under a small layer of Quaternary soils (analysis of archival research boreholes from the Polish Geological Institute), and on the basis of geophysical research already performed later in the collection resistivity ranges of the studied Triassic formations (Fig. 6).

It was found that the recognition of the subsoil in terms of the presence of anomalous zones (voids) to a depth of 30-60 m will be sufficient. Based on many years of local experience and research, it can be concluded that a rock mass with a stable structure (without disturbances) within 30-40 m below ground level is considered safe and should not adversely affect the safety of the foundation of most construction investments.

The above, of course, will depend on many other variables, such as: leaching intensification, karstification of the above-mentioned carbonate rocks, water dynamism, existing or completed multi-seam mining of hard coal under Triassic formations, the above results in the possibility of reactivation of old coal goafs - destructive and affecting the stability Triassic orogen (described in more detail), and others.

The applied geophysical methods and depth ranges also allowed for the verification of the condition of the Carboniferous orogen.

This allowed for a deeper verification of the condition of the orogen, its assessment and a relative forecast of the impact on Triassic rocks.

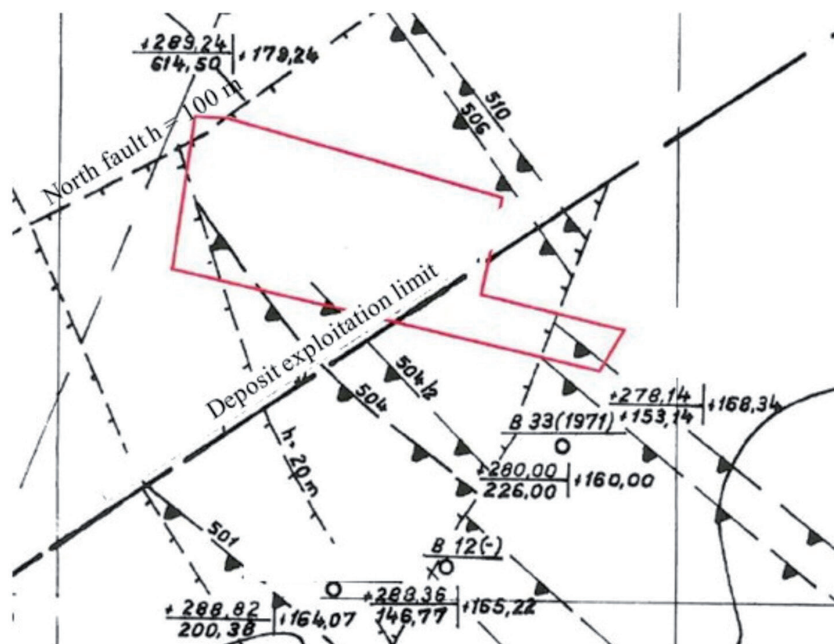


Fig. 3. Carboniferous roof in the research area A with the marked course of the "North" fault and outcrops of seams 501, 504, 506, and 510.

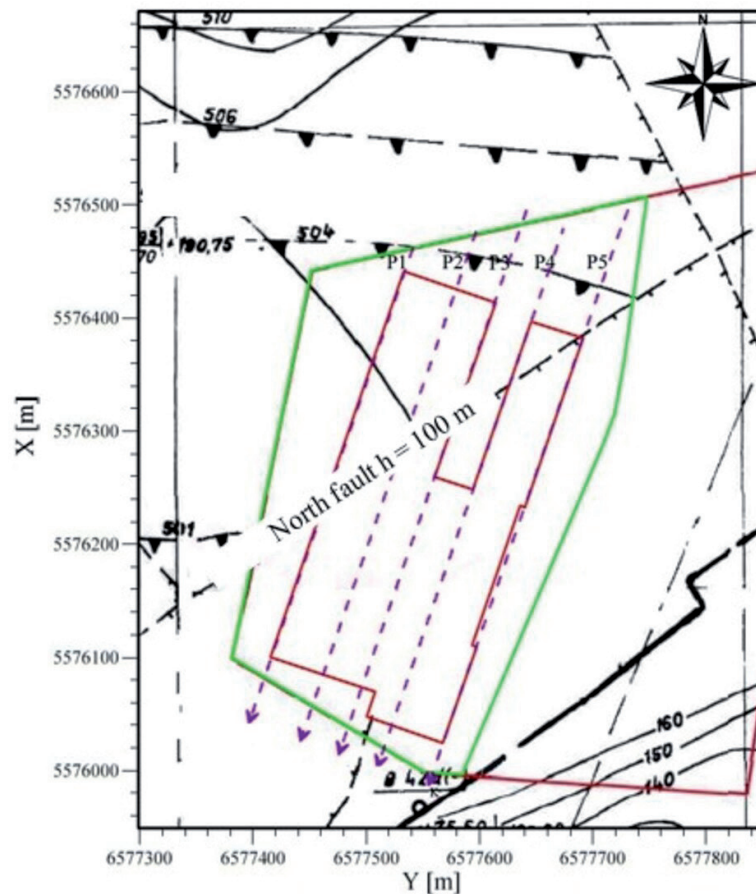


Fig. 4. Carboniferous roof in the research area B with the marked course of the “North” fault and outcrops of seams 501, 504, 506, and 510.

However (as it was shown), the largest anomalies indicating the possibility of voids, or zones of loosening, thickening - occurred in the zone of carbonate rocks.

Therefore, the subsequent verification of anomalous zones in the form of control and injection wells was performed in the depth range (20-35 m), the so-called safety ledges, in the zone of Triassic rocks prone to karst phenomena.

Nevertheless, in consultation with all participants of the investment process, it was decided on the scope of research and their verification presented in this article.

Mining History

Directly below site A mining was carried out with the roof caving for a total thickness of about 7.2 m - 7.3 m in the middle of the 20th century. Mining in three seams took place in the depth range of 120 m - 150 m, and another one at a depth of about 600 m. On the eastern part of the A area surface, a subsidence trough developed to a maximum depression of about 10 m to the surrounding area. In the B area, mining was carried out intermittently throughout the second half of the 20th century. Five seams were mined using the roof caving method at a total thickness of about 11 m. Another one seam of an average thickness of

5.3 m has been extracted with hydraulic backfilling. Except for one seam with a thickness of 1.4 m lying at a depth of more than 600 m, the remaining seams are in the depth range of 160 m to 340 m. The relatively shallow depth of these coal seams resulted in significant deformations in the rock mass and on the ground surface during subsidence troughs formation. Both areas were also within the range of extraction influences carried out in the neighborhood.

Taking into account the average values of the ground surface subsidence coefficients for the rock mass in the conditions of the GZW and the mining techniques used, it can be assumed that as a result of underground hard coal mining, the land surface in the A region decreased by about 6 m in the B region by about 9 m compared to original topography.

Results

Results of the Conducted Geophysical Research in the A Area

The tests carried out using the two-level electrical resistivity imaging profiling (ERP) method in the medium gradient system using measuring sections

of the electrodes with the lengths $AB = 270$ m and $AB = 540$ m in a 5-meter grid of measuring points.

The distance between electrodes $AB = 270$ m has been selected to achieve increased readings resolution. Their depth range determined based on many years of experimental work is estimated at 65 m \div 70 m. In the considered case, the measured differences in the resistivity are related to discontinuities in the layers of carbonate rocks.

The second, larger measurement spacing $AB = 540$ m was adopted for hazard identification in the Carboniferous layers. This survey enabled the visualization of changes in the rock mass resistivity at a depth of about 125 m to 135 m. On its basis, the identification of anomalous resistivity zones resulted from mining operations in thick seams 506 and 510, lying at a depth of 120 m to 160 m, has been conducted.

The Carboniferous roof map (Fig. 3) demonstrates that practically the entire area of the planned investment is within the former extraction of the seams 506 and 510, and also in the southern part of the investment area, seams 504 and 504/2. Concerning the area in question, the underground voids of significant volume may still exist after past mining operations. Underground voids may be direct remains of mining workings or suspended (migrating) voids formed in the overburden during the successive collapsing of unstable roof rock strata, causing a void to gradually move towards the surface that finally appears on the ground surface in the form of a discontinuous deformation.

The main criterion for separating anomalous zones in the measurement field was the average value of apparent resistivity. Any deviation from the mean resistivity in the studied rock medium, in the form of a significant increase in this value or a considerable decrease, is taken as anomalous zones. Table 1 presents a summary of the resistivity values obtained due to the conducted electrical resistivity imaging measurements.

Results of measurements obtained with electrode spacing $AB = 270$ m indicated the presence of a high-resistivity anomalous zone. For the spacing $AB = 540$ m, both low- and high-resistivity anomalous zones have been found, Fig. 5.

Low-resistivity zones indicating the migration of water or the occurrence of looseness filled with water show a significant decrease in this value on resistivity maps. High-resistivity zones are water-free, dry, or air-filled structures, such as voids or cavings. In the case of the spacing $AB = 540$ m, they could be the remains of mine workings and collapsed roofs because the resistivity isolines reflect the directionality of the NW-SE carried out in this area.

As a result of the analysis of the drilled boreholes, two geological structures on the A area have been identified. In the western and eastern parts, hard limestone rock is marked at a shallow depth (holes 1, 2, 3, 7, 9, 13, 15, 19, 20, 21, 25, and 27, except for holes 8, 14, and 26), while in the middle part, the limestone occurs only below the thick cohesive and plastic rock

Table 1. Range of resistivity values observed during electrical resistivity imaging tests in area A.

Apparent resistivity [Ω m]	Electrode spacing $AB = 270$ m	Electrode spacing $AB = 540$ m
Minimum	22	3
Maximum	652	268
Average	152.6	85.3

formation. Therefore, the central part is a regular sinkhole (a subsidence trough). It can be assumed that tensile forces dominate in the trough, as is the case in the fault zone. This fact causes the overlying limestone formations to be agitated and cracked because the rock shows no resistivity to tensile forces. Reduced resistivity values mark tectonic faults on the ERT map due to their possible failure or filling the sliding plane with clay. Based on the results of geophysical studies, in correlation with the map of the bedrock roof, it can be seen that in this basin, low-resistivity anomalies occur. They are related to the free migration of fine particles washed out into the rock mass (suffosion causing disintegration of the carbonate medium). Apart from the basin, there are high-resistivity anomalies present. One can expect loosening of the rock mass and even the presence of voids in the maximums of anomalies, also near the surface (hole No. 6) due to the principle of overlapping high-resistivity anomalies in the depth interval.

Fig. 5 shows the maps of the apparent rock mass electrical resistivity imaging distribution in the study area. In the Triassic layers, there are evident high-resistivity anomalies present in the western part of the study area, with a zone of exceptionally high resistivity lying at the southern edge of the study area, slightly outside the outline the designed building. Visible zones of high-resistivity anomalies occur in carbonate rocks at a depth of 25 m \div 30 m and in Carboniferous rocks at a depth of 125 m \div 135 m, Fig. 5.

As a result of mining works, a subsidence trough developed (Figs 3 and 4). It means that the mine voids in seams 506 and 510 have been at least to some extent filled up with loose material from the subsurface layer of fine-grained formations in the overburden or the Carboniferous strata. This effect results from the different strength properties of carbonate and Carboniferous rocks. Rocks with lower tensile strength, more brittle, and prone to disintegration into separate and displaced blocks (cavings) constitute the direct roof of the coal seams up to the Triassic floor, easily deformed and fall into workings and mined out voids.

Further displacement of voids in the rock mass towards the ground surface stopped in compact carbonate rocks. As a result, permanent voids and loosening appeared in these rocks. Such a course of deformation phenomena also significantly affects the local hydrogeological conditions. For example,

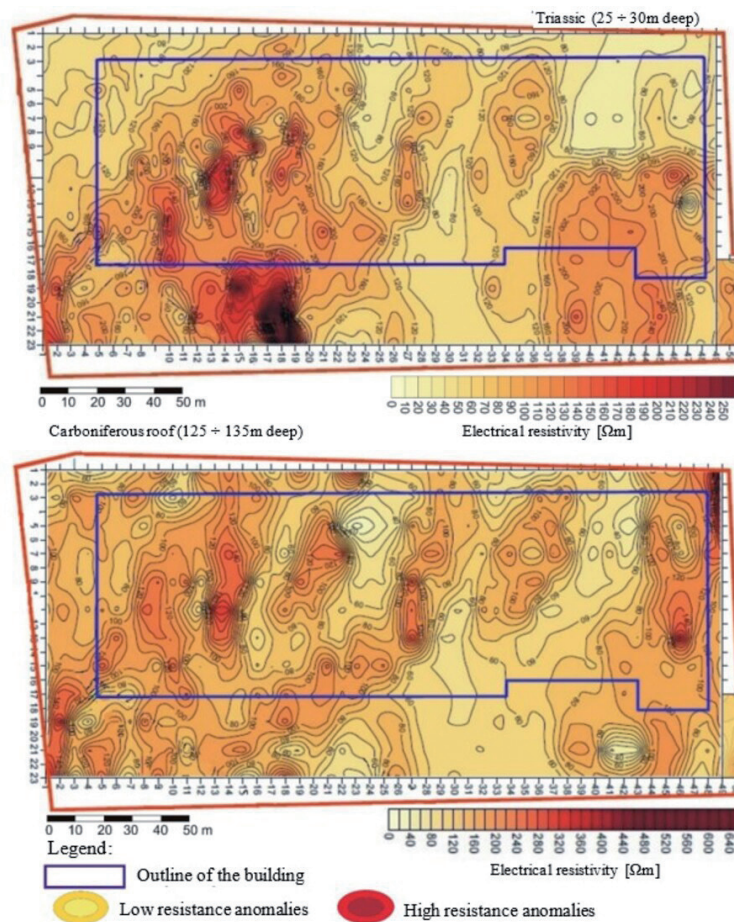


Fig. 5. Distribution of electrical resistivity imaging anomalies in the Triassic (25÷30 m deep) and Carboniferous (125÷135 m deep) layers in the A area.

the Triassic layers show more water failure than the underlying Carboniferous formations, suggesting that they maintain an isolated groundwater level, in contrast to the Carboniferous layers, characterized by higher electrical resistivity imaging resistivity.

Analysis of the maps of the electrical resistivity imaging distribution for the depths of 25-30 m and 125÷135 m concludes that high-resistivity anomalies are higher in value and more regularly distributed in the limestone overburden than at a depth of coal extraction.

Results of the Conducted Geophysical Research in the B Area

To achieve the set goal in area B, 5 measurement profiles were made, with a length from 444 m to 540 m, on a total distance of 2,476 m. Due to the research problem, electrical resistivity imaging tomography has been selected. Apparent resistivity measurements were made using the dipole-dipole spacing. This system is sensitive to changes in resistivity resulting from vertical structures that differ in conductivity and is recommended for the performance of induced polarization. Due to technical possibilities, each

measurement was performed with a maximum profile length of 252 m. The maximum length directly affects the penetration depth obtained. Based on many years of experience, it is estimated that the maximum depth is 20-25% of the length of the measured part of the measurement profile. Therefore, the maximum obtained penetration depth was estimated at 46 m.

The measured values were used to calculate the resistivity using iterative methods. As a result, the inverse problem has been solved using the specialized RES2dinv software. In addition, the resistivity measurements were supplemented with the area's topography, thanks to which the inaccuracy of solving the inverse task was reduced. Point solutions obtained by inversion were used as the basis for modeling a two-dimensional distribution of resistivity. Logarithmized values have been adopted due to the considerable range of the obtained values (from several to several thousand Ωm). This process was carried out using an acceptable geostatistical method – kriging.

Geological information indicates a layer with a thickness of 100 m to 150 m of Triassic and Quaternary overburden over the Carboniferous rock massif. The maximum depth of penetration, amounting to 46 m, allows for characterizing the electrical resistivity

imaging properties of the bedrock within the Triassic rocks and the developed Quaternary.

A detailed geological map of Poland and materials from geological surveys indicate the possibility of Triassic outcrops in limestone, dolomites, and marls. In addition, many years of research have allowed Authors to statistically develop the resistivity ranges of individual sedimentary rocks (Loke 2016). Fig. 6 shows the ranges and the scale of resistivity used, along with the marked boundaries, for particular rock formations.

Marl's low-resistivity properties result from the presence of clay minerals in the rock. Limestone resistivity, ranging from several dozen to several thousand Ωm , result from the difference in the formation of the bedrock (marly limestone, porous limestone, plate limestone, etc.), water presence, and erosive processes. The Dolomites, made of limestone, are characterized by higher resistivity values to the previously considered deposits.

An important factor influencing the obtained values is the karst process leading to erosion of the bedrock. Due to the infiltration of water within the bedrock, a decrease in resistivity takes place. The reduced resistivity (in relation to the recorded trend) may also result from the deposition of clay material within the eroded substrate. In this case, the original bedrock is filled with sedimentary material. When eroded limestone is not filled with water (as a result of lowering groundwater levels), an increase in resistivity is observed compared to the recorded trend. The voids formed during the leaching of rock material are filled with air, which is a high-resistivity medium.

Lower resistivity values characterize diluvial sediments due to the mixing of eroded bedrock with the Quaternary material. In many cases, the conductivity properties of the subsurface zone correlate strongly with

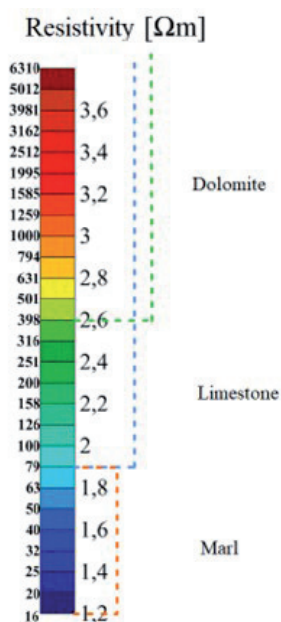


Fig. 6. Resistivity ranges of the studied Triassic formations.

the topography of the area. On the results of electrical resistivity imaging tomography, diluvial sediments are visible in the form of a low-resistivity layer of considerable thickness.

For electrical resistivity imaging measurements, it is necessary to determine the characteristic values of the tested subsoil and designate anomalous zones that have arisen due to the subsoil's erosion. Diversification of resistivity is the basis for establishing zones potentially dangerous for the planned investment.

The results obtained during data processing were used to create two-dimensional distributions of resistivity (Fig. 7) and a flat resistivity distribution at the selected shear level, Fig. 8. In addition, each electrical resistivity imaging section was supplemented with the boundary of the area covered by the investment, the contour of the designed object, the Northern fault, and the selected location of the research and injection formations, the information of which details the data on the geological structure of the studied area. The boundaries of the deposits with different electrical resistivity imaging properties have been marked on the obtained resistivity distributions. As an example, Fig. 8 shows the distribution of resistivity at +270 m above sea level. (about 20 m above the ground surface).

Injection/Filling Works

The filling works were carried out as a result of finding significant loosening in the rock mass during drilling works (after geophysical research) - no voids in the rock mass. The protective works were focused on sealing and solidifying the medium by filling it by gravity - injection under hydrostatic pressure of the grout.

The main purpose of soil conditioning grouts is to completely fill the crack zone and seal the rock mass. In the existing conditions, the injection took place indirectly through a system of cracks in the rock mass and the degree of penetration depends on their size and hydraulic connectivity. To ensure maximum penetration, the treatment mixture should have good crevice penetration properties and fluidity enabling pumping with a pump system. In order to ensure maximum migration of the mixture, it was decided to use a product based on fly ash (a product after burning coal/lignite, with good binding/pozzolanic properties), with the coefficient w (water) / c (solids - fly ash) = 0.5 - 0.6. On the assumption:

specific gravity of the product: $\gamma = 2,45 \text{ g/cm}^3$

grout volume: $V = \frac{1}{\gamma} + w/c$ then $V = \frac{1}{2,45\gamma} + 0,5 = 0,908 \text{ t/m}^3$

Thus, from 1 ton of a product with a specific gravity of 2.45 g/cm^3 , we get the coefficient water $w/c = 0.5$ slurry with a volume of 0.908 m^3 .

It is mentioned that in order to achieve the recommended compressive strength of 5 MPa after 28 days of seasoning, other additives accelerating

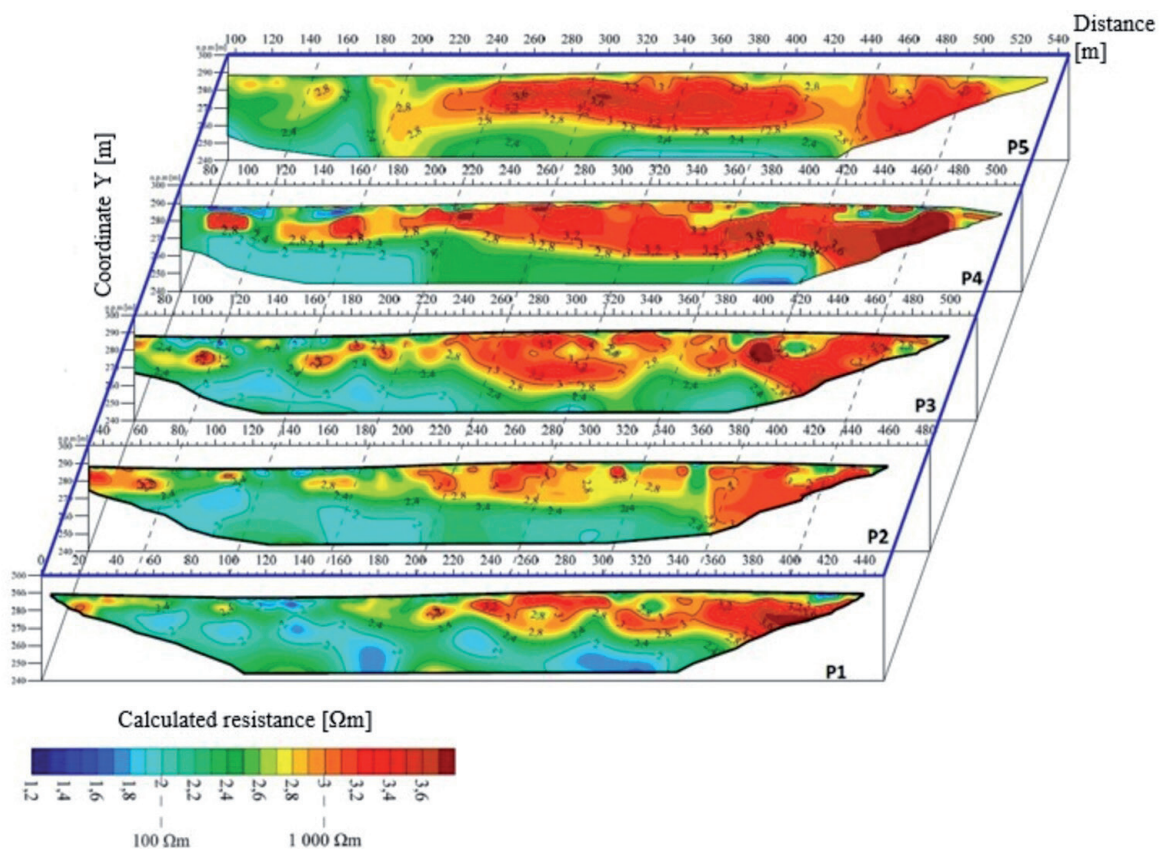


Fig. 7. Summary of the results of electrical resistivity imaging tomography in area B.

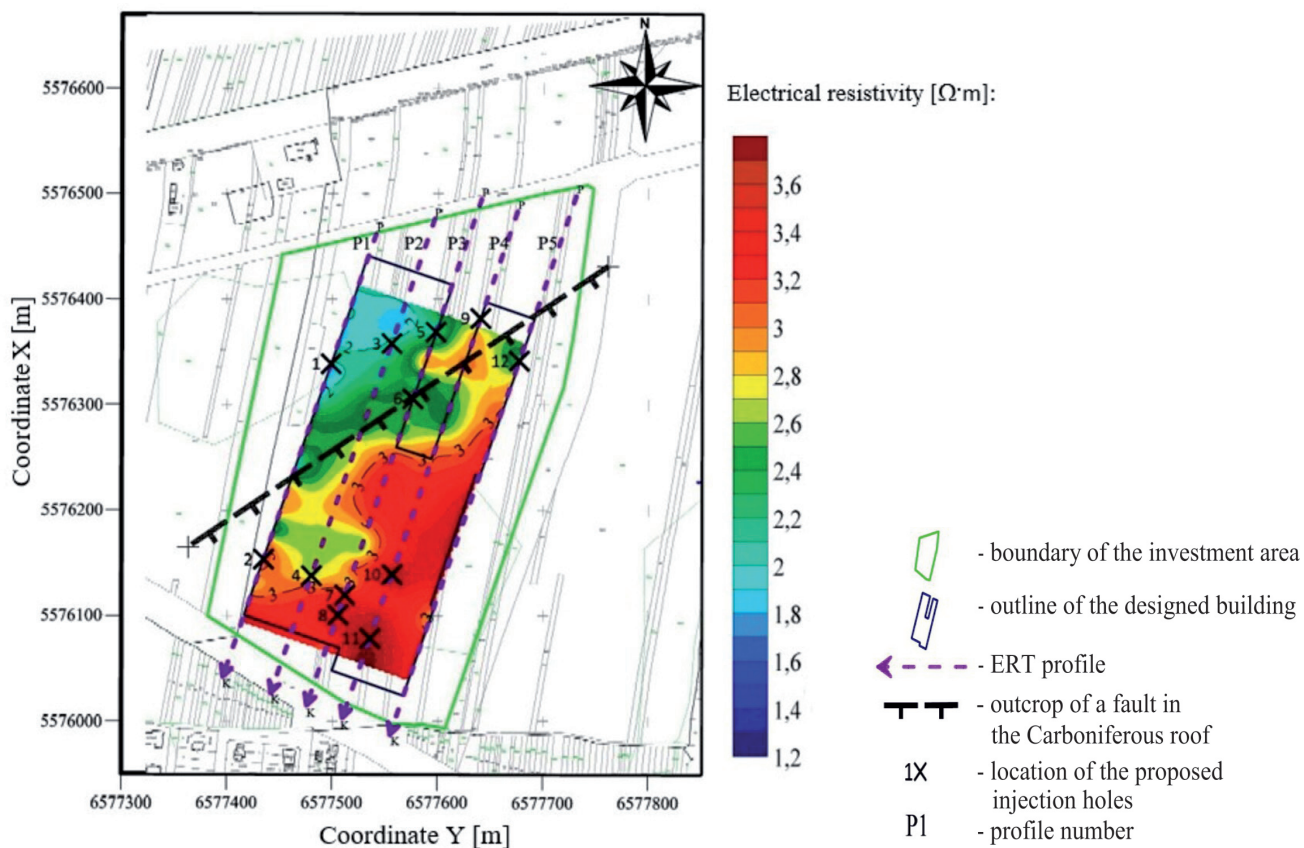


Fig. 8. Distribution of the calculated resistivity at the ordinate of 270 m above sea level. (about 20 m below ground level) in area B.



Fig. 9. General view of the completed drilling and injection process (copyright photo).

the setting process, e.g. cement, can also be added to the stabilizing mixture. In addition, to obtain the recommended strength, the mixture can also be thickened by changing the w/c ratio. The above may, unfortunately, lead to a decrease in the parameter of the mixture flow, and thus significantly reduce the effectiveness of filling the zones of loosening, thickening, or even correct filling of the detected void.

The mixture was filled through the inlet of the hole equipped with a casing pipe injection until loss of absorbency. Grout injection was completed in each of the holes at a distance of about 0.5-1.0 m below the ground surface (Fig. 9).

Drilling and Filling Works in Area A

Based on the results of electrical resistivity imaging tests, 16 research and backfill holes were drilled, located at points of extreme electrical resistivity values. First, the holes were drilled to a depth of 35 m using a drill bit with a diameter of 200 mm to the bottom of the layers of loose formations. Then drilling was continued using a coreless mechanical-rotary method with drilling mud and a 137 mm diameter cutter bit. After passing through the rock weathering and reaching the solid rock, casing pipes were placed in the holes and sealed by plastering. Fig. 10 shows the arrangement of test and injection drill holes.

Based on the results of electrical resistivity imaging tests, 16 research and backfill holes were drilled, located at points characterized by extreme electrical resistivity values. The holes were drilled to a depth of 35 m using a drill bit with a diameter of 200 mm to the bottom of the layers of loose formations, then drilling was carried out using a mechanical-rotary method on a coreless water drilling mud with a 137 mm diameter cutter bit. After passing through the rock weathering and reaching the solid rock, casing pipes were placed in the holes and sealed by plastering. The arrangement of test and injection holes is shown in Fig. 10.

In the study area's geological profile, loose Quaternary formations with a thickness ranging from about 0.4 m to 4.9 m occur. Below them, a layer of weathered rock and rubble constitutes the top of the Triassic layers. The thickness of this layer is approximately 2.5 m on average. Below, up to the bottom of the borehole, solid carbonate rocks are

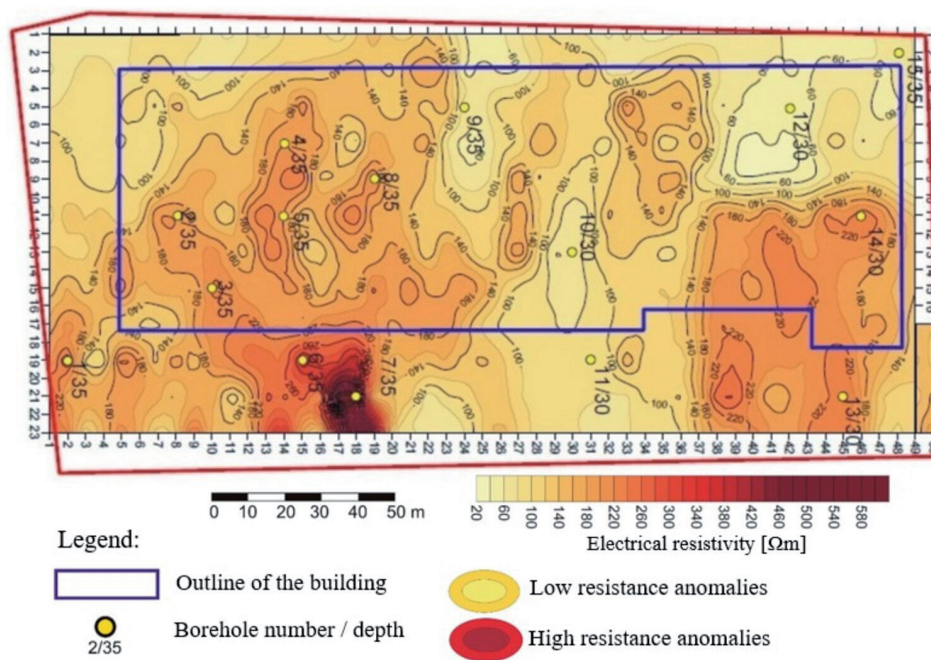


Fig.10. Distribution of apparent electrical resistivity imaging anomaly in the depth range up to 25÷35 m after the injection works with the location of the holes in the area A.

represented by limestone, dolomites, and heterogeneous marls.

Drilling works show the presence of local loosening and cracks of varying severity. Changes in rock compactness can be read from the timing of drilling progress. Differences in drilling progress between individual meters indicate the degree of variation in rock compactness and looseness and voids.

The drilling results showed that the cracked and partially weathered roof layers are characterized by high variability in the drilling progress. First, from about 11 m to 17 m, there are very dense and homogeneous deposits present. Then the distinct weakening of the rocks with a very strong loosening from 20 m to 22 m indicates a large fracture zone. Within this zone, the increased absorbency of the injection mixture was expected.

In nine boreholes, a continuous outflow of drilling mud starting in the range from 5 m to 35 m to the bottom of the boreholes occurred. In addition, all boreholes had isolated, several dozen cm thick, drilling mud disappearing zones, encountered from the Triassic roof to the bottom of the boreholes, with no apparent relationship to the type of drilled rocks.

The lack of visible signs of the occurrence of voids during drilling does not allow to confirm their presence, and the sudden local drop of the drill string (usually 0.2 m - 0.3 m) was marked as very strong loosening. Thus, it results from geological conditions and indirectly from mining extraction.

The carbonate formations of the Triassic form a fissure-karst aquifer with a water level stabilizing at a level from 9.3 m to 20.2 m below sea level, depending on the morphology of the site. The nature of the water level favors creating favorable conditions for water circulation, which are the leading cause of the drilling mud disappearance. Probably the marl complex drilled in the bottom of the dolomites insulates the aquifer. A high level of water remaining in the boreholes may prove that the insulation is continuous and the mine workings do not drain the water.

The whole area, as a result of mining operations, settled over time. During this process, the less dense rocks became intensely fractured. The absence of voids and a constant high groundwater level may mean that the fracture zone penetrates the overburden, but the caved zone does not reach the overburden boundary. Considering the time that has passed since the end of mining works, the deformation processes of the rock mass and the ground surface have probably been completed, ensuring the stability of the rock mass.

The occurrence of loosening zones and outflow of drilling fluid only slightly correlates with the distribution of the most intense low- and high-resistivity anomalies zones shown on the map of electrical resistivity imaging distribution of the test area at a depth of 25-30 m.

Four holes were selected for injection, in which intense fluid escapes during drilling occurred.

The remaining holes were cemented and backfilled. The three injection holes were located in the western part of the A area in low-resistivity anomalous zones (10, 12, and 15, see Table 2 and Fig. 10). In the western part, the only hole in the zone of increased (but not extremely high) resistivity was the no. 5 drill hole.

The injection mixture was introduced into the voids by gravity through previously made boreholes. In this method, the migration of the filling mixture into the voids takes place under the influence of the hydrostatic pressure of the mixture column, the maximum value of which (when the hole is filled completely) is the product of the column height and the density of the mixture [5].

The total absorptive capacity of all holes was approximately 93.7 m³ of the mixture. The volumes of the filling mixture absorbed by the individual injection ports in area A are listed in Table 2. The distribution of electrical resistivity imaging in the Triassic layers at a depth of 25÷30 m after backfilling works is shown in Fig. 7.

Analysis of the distribution of apparent electrical resistivity imaging on the Triassic map at a depth of 25÷30 m before and after the injection works, leads to conclusion that the sealing of the area around holes No. 10, 12, and 15 located in the eastern part of the investment site, caused a slight increase in apparent electrical resistivity imaging by about 100÷120 Ωm (see Fig. 5 and 9), evenly throughout the eastern part of the area under consideration. The injection of the area of hole No. 5, which absorbed only 12 m³ of the mixture, led to a significant increase in apparent resistivity in the entire western region of high-resistivity anomalies, defined by the location of boreholes 2 to 8. In addition, it is worth noting that the injection of voids through hole No. 5 caused an increase in apparent resistivity within a radius of about 40 m.

Drilling and Filling Works in Area B

From the first geophysical works in 2018 until the commencement of drilling works in early 2020 on the surface of area B new discontinuous deformations appeared, Fig. 11, which mostly coincide with the course of the Northern fault in the Carboniferous rock roof at a depth of approx. 110 m below sea level. Due to this fact, two additional injection holes have been drilled in the vicinity of the deformation sites (No. 13 and 14) and on the outer contour of the designed building (No. 15) in the NE corner above the fault, Fig. 12. Thus, a total length of 328.5 m of drilling was executed.

The drilling works were carried out by making holes with a diameter of 180 mm in the Quaternary overburden and a diameter of 143 mm in the Triassic layers using a grinder. To protect the borehole against self-backfilling and to carry out treatment works freely, the borehole was cased in Quaternary and weathered rocks using PVC pipes of 160 mm diameter. Then, the bedrock was drilled through using a grinder and a drilling mud system with a closed circuit.

Table 2. The depth of the drilling mud decay, the volume of injection mixture absorbed by the holes in area A and the amount of binder used.

Hole No.	Hole depth [m]	The depth of complete decline of the drilling mud [m]	The weight of the binder used [Mg]	Injection volume [m ³]
5	35	16.6	12.0	10.9
10	30	9.8	25.3	23.0
12	31	9.2	30.1	27.3
15	35	4.5	35.8	32.5
Total:			103.2	93.7

Together with the results of electrical resistivity imaging, the performed geological tests indicate variable physical properties of the tested bedrock. In many places, the rock mass shows significant fractures, which were revealed during drilling. The results of drillings made in the northern part of the B area show much larger fractures than in the southern part.

Moreover, the bedrock in the northern part, located directly below the Quaternary formations, is strongly influenced by erosive processes. In borehole no. 1 (the location of the holes is shown in Fig. 8 and 12), the presence of a strongly eroded rock mass with numerous fissures was noted, the bottom of which was defined at a depth of 13.7 m below sea level. In borehole No. 5 in the depth range from 2.8 m to 6.8 m below sea level, a heavily eroded layer filled with clay or mud has been found. In borehole No. 6, the presence of eroded bedrock has been observed in the depth zone between 2.95 m and 26.1 m below sea level, below which the solid bedrock has been finally met. In borehole no. 12, numerous cracks have been found to a depth of 26 m below sea level.

In the holes in the southern part of area B, the rock layers directly below the Quaternary overburden show

a lower degree of eroding than in the holes located on the northern side of the B area. In all the holes made in the southern part, hard bedrock was recorded directly under the overburden. In borehole No. 4, this layer is visible between 4.7 m and 8.8 m of depth below sea level. In hole no. 7, the roof is covered with a hard rock layer in the zone between 2.35 m below sea level and 12.3 m below the sea level and also in a borehole no. 11 between 1.5 m and 7.6 m below the sea level. In this layer, occasionally, small cracks filled with clay material were noticed.

During the geological work performed, three voids were found. In the area of borehole 1, at a depth of 5.8 m, a karstic void was found, the bottom of which was 0.7 m below. Another void was located in borehole No. 6, at a depth between 16.1 m and 16.3 m below sea level. The last recorded void was found at a depth of 16.5 m - 16.7 m below sea level in a borehole no. 11.

Because in all 15 holes, cracks and loosening were noted, complete or partial disappearance of the mud while drilling the boreholes occurred, and the above-mentioned voids have been found; treatment works were undertaken to fill up the discontinuities with a geotechnical binder.



Fig.11. Discontinuous linear deformation along the North Fault in area B (copyright photo).

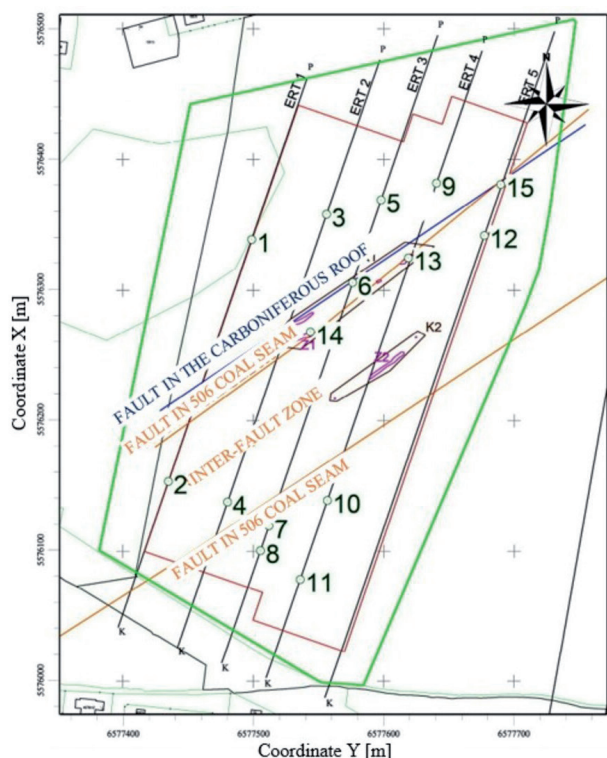


Fig. 12. Distribution of injection holes and surface deformations in the B area.

For injection works, Grunton and Duraset mineral binders were used alternatively, depending on the possibility of using them in a given location. Duraset binder application is discussed in the description of the injection works in area A. Grunton is delivered to the site in the form of a mixture ready to use, which allows its application without access to water and electricity.

The absorptive capacity of the individual holes varied considerably (Table 3), and their size depended on the degree of rock substrate degradation. The highest absorptions were recorded in the holes located in the zone where deformations of discontinuous terrain

surfaces are located (Fig. 11). In the course of the linear deformation, local erosion gutters were documented, to which the geotechnical binder was fed directly from the concrete truck. As a result, the linear deformation is relatively narrow and scarred over most of its course.

The measure of complete sealing of the injection hole with a geotechnical binder is the loss of absorbency manifested by the outflow of the medium onto the surface of the ground. All technological boreholes submitted to the injection procedure had completely lost their absorbency. A summary of the amount of injection mixture used in individual geotechnical holes as well as the amount of binder used to fill the gaps on the surface (linear deformations) is presented in Table 3.

Discussion

Both areas are close to each other and represent very similar geological conditions. In both, a Quaternary diluvium of variable thickness was found, under which the Triassic carbonate massif is found. In all the exploratory wells drilled in A and B areas, eroded and fractured zones within the dolomite formations were encountered.

From the point of view of the mining extraction, areas A and B differ slightly, which may have an impact on the risk of discontinuous deformations in the bedrock and on the ground surface. In area A, the scope of extraction directly below its surface includes a set of coal seams of a total thickness of about 7.3 m with a collapse of the roof (forecasted ground subsidence of 6 m). In comparison, in the area B, the mining was more intensive. An 11 m thick layer of coal with a collapse of the roof and 5.3 m with hydraulic backfilling was mined out, giving an approximate value of lowering the ground surface to about 9 m.

Area A is slightly affected by faults in the Carboniferous. The North Fault with a throw of 100 m runs at its north-west edge (Fig. 3), while it passes through the center of area B together with the

Table 3. Summary of the volume of injection mixtures used in the treatment works in area B.

Hole No.	Depth [m]	Fill volume [m ³]	Hole No.	Depth [m]	Fill volume [m ³]
1	25	18.3	10	10.5	1.5
2	20	4.4	11	17	2.1
3	20	18.5	12	36	8.5
4	20	3.5	13	20	23.1
5	25	7.3	14	20	19.3
6	30	22.5	15	20	4.2
7	25	4.6	Crack Z1	-	6.0
8	20	4.0	Crack Z2	-	7,1
9	20	3.6			

second, minor fault, creating a wide fault zone (Fig. 4 and 12), within which the discontinuous deformations of the ground surface (Z1 and Z2, Fig. 12).

In the geophysical research of area A, the method of two-level electrical resistivity imaging profiling in the medium gradient system with the electrode spacing of 270 m and 540 m was used, which made it possible to obtain maps of the resistivity distribution of the medium at a depth of about 25 m - 30 m and 125 m - 135 m, respectively. Research was carried out with the use of electrical resistivity imaging tomography in the dipole-dipole system in five sections up to a depth of about 46 m. The results of the measurements are sections in five measurement lines and maps of the test area planes determined by interpolation from the obtained vertical sections to any depth within the range of the measurements.

Analysis of the type and structure of information obtained with the use of both variants of the electrical resistivity imaging method leads to the conclusion that the electrical resistivity imaging profiling applied in the area A, carried out for two levels, gave much less meaningful information than the electrical resistivity imaging tomography carried out in the area B. In particular, the assessment of the rock mass properties at a depth of the Carboniferous roof (about 12 m below the sea level), located significantly below the depth of injection holes and the range of impact of loads of the designed building structure, brought little cognitive value. On the other hand, the detailed tomography of the rock mass performed in area B gave a three-dimensional image of the rock mass within the range of 46 m, sufficient to assess the geological conditions within the layers that could be subjected to injection treatments and that are within the scope of the impact of the designed building.

A potentially more practical solution in the case of electrical resistivity imaging profiling would be to adopt shallower levels of the measurement planes, within the depth of the injection holes, which could better optimize their position to the zones of cracks and loosening possible for infiltration and not lying at greater depths.

Due to the lack of deformation phenomena visible in the field, the scope of injection works in area A was limited to the holes in which the complete disappearance of drilling fluid was found during drilling, and electrical resistivity imaging tests showed low apparent resistivity of the medium. Taking into account the fact that in the area B, where all the holes were injected, the absorption capacity of the holes located in the zones with high resistivity of the medium was deficient, it can be concluded that carrying out injections in zones with high apparent resistivity is not justified.

The average value of the absorptive capacity of the injection wells located in the zones of low apparent resistivity of the medium was 23.4 m³ in area A and 20.3 m³ in area B. Therefore, these values are similar. On the other hand, the average volume of the injection taken by the holes in the zones of high apparent

resistivity in area B was 4.4 m³, and the absorptivity of individual holes ranged from 1.5 m³ to 8.5 m³. Therefore, the average absorptivity of a hole in the zone of high apparent resistivity of the rocks was 4.65 times lower than in the low apparent resistivity zones in area B.

For injection works in both areas, a strong correlation was found between the absorptive capacity of individual boreholes and the local value of apparent resistivity in the zone of the borehole location, intensity of drilling fluid escapes during drilling, and the extent and degree of erosion and fractures of the loosened rock structure.

Conclusions

The examples of geophysical surveys of the area of the planned investment and the protective measures carried out as a result of it, presented in this article, show the mechanism of eliminating geomechanical threats to the ground surface and shallow rock layers from mining extraction carried out in the conditions of the presence of a thick cover of Triassic formations in the carbon overburden exposed to erosive processes.

From the point of view of construction in post-mining areas, it is essential to eliminate the possibility of deformation of the ground surface and the formation of loosening in the subsoil, which adversely affects its load-bearing capacity. In the case when the building is seated on carbonate rocks, the leading cause of adverse effects on the surface should be mechanical suffosion - migration of fine grains of the overburden to fissure-cavern voids in the mass of carbonate rocks, karst processes, and the presence of active tectonic structures, in this case, significant fault.

The activity of the fault running through the B area manifests itself in the generation of significant deformation movements in the carbonate medium, which results in the occurrence of linear deformations in the form of fissures and field faults. The activity of large faults results from extensive, multi-seam mining operations carried out over a large area by the numerous mines operating in the region. While the calming of deformation movements causing the formation of subsidence basins lasts from several to several years after the end of mining works, the slow movements of large masses of the rock mass, more reminiscent of orogenic activities, may last much longer. During this time, there may be movements of rock masses on the fault plane, the advective flow of small rock grains from higher parts of the rock mass causing the formation of voids and loosening, and in the case of excessive stresses on the fault plane and accumulation of elastic energy due to blockage of rock masses, also strong seismic phenomena.

Analysis of the two case studies of areas exposed on the discontinuous deformations hazards presented in this paper shows that the presence of active faults

is a more severe threat to the ground surface than the former mining operations, in a situation where a significant time elapsed since their completion and their depth exceeds the depth limit of the keeping of entire mine workings and cavings in the stable conditions for very long periods, depending on local geomechanical properties of the rock mass.

The formation of cracks and loosening zones and large-size voids are favored by rock mass deformations resulting from the coal mining in the Carboniferous rocks lying below.

The conducted research has shown that the absorptivity of individual test and injection wells can be inferred primarily based on the drilling process by observing the drilling fluid escapes, drilling progress, and the structure of the drilled rock. In addition, geophysical studies of the subsoil structure, in the profiling or electrical resistivity imaging tomography version, allow determining the locations of loosened zones (low-resistivity anomalies), which may be the basis for selecting the number and location of the test and injection wells.

Important information for the location of research and injection wells is the presence and location of active tectonic structures, information about which was obtained within the cartographic data related to historic mining operations in the studied areas.

Comparing the two types of electrical resistivity imaging tests carried out in areas with a very similar geological structure, geomechanical properties, post-mining history, and other factors determining the results of electrical resistivity imaging measurements, it can be concluded that to assess the conditions for the foundation of buildings, electrical resistivity imaging tomography is a more advantageous method of testing, providing a detailed three-dimensional image of the studied rock mass in-depth range covering injection works carried out in the zone of impact of loads on building structures and vastly exceeding this range.

It can be mentioned here that in connection with the planned investment, it is also necessary to ensure the tightness of underground pipelines carrying liquid media (water, sewage, etc.) and prevent the inflow of water (e.g. rainwater from the roof, snow storage). Possible unsealing of the installation may cause a strong migration of water into the orogen (intensification of karst phenomena in the layer of carbonate rocks and intensification of fracturing of fractured Carboniferous rocks), which in turn may lead to the development of discontinuous or, in particular, continuous deformations on the surface.

The above was the essence of this article.

Acknowledgment

The authors would like to thank the GEOSOLUM company for providing the equipment and helping in

conducting the field research and processing of the data.

Conflicts of Interest

The authors declare no conflict of interest.

References

1. DEBEGLIA N., BITRI A., THIERRY P. Karst investigation using microgravity and MASW: application to Orleans, France. *Near Surface Geophysics*, **4**, 215, **2006**.
2. HUSSAIN A.M, ZHANLONG C., ZHENG Y., SHOAI B M., SHAH S.U., ALI N. AFZAL Z. Landslide Susceptibility Mapping Using Machine Learning Algorithm Validated by Persistent Scatterer In-SAR Technique. *MDPI – Sensors*, **22** (9), 3119, **2022**.
3. XIAOMEI G., YUNHU X., WENBANG G., LIXING Z., YINGGA W, RUIPING Z. Comprehensive Evaluation of Soil Quality: a Case Study from a Semi-Arid Area Experiencing Coal Mine Related Subsidence in China. *Polish Journal of Environmental Studies*, **30** (5), **2021**.
4. YINGGA W., XIAOMEI G., DANDAN Z., RUIPING Z. Changes in Soil Physical and Chemical Properties after a Coal Mine Subsidence Event in a Semi-Arid Climate Region. *Polish Journal of Environmental Studies*, **31** (3), **2022**.
5. LI J., HERONG G., RONGJIE H., LUWANG C., YUTING X., HONGXIA F., HAO Y., MEICHEN W. Analysis of Heavy Metal Sources and Health Risk Assessment of Typical Coal Mine Collapsed Lakes in Huaibei Coalfield, Anhui Province, China. *Polish Journal of Environmental Studies*, **29** (5), **2020**.
6. IJAZ M, AKRAM M., AHMAD S.R., KHAN W.U., THYGERSON S.M., NADEEM F.A. Dust Generation and Respiratory Impact of Underground Coal-Producing mines in Pakistan. *Polish Journal of Environmental Studies*, **29** (5), **2020**.
7. STROZIK G. Filling underground cavities in rock mass disturbed by mining. Publishing House of the Silesian University of Technology, Gliwice **2015** [In Polish].
8. STRZAŁKOWSKI P. Shallow voids in mining areas and the possibility of sinkholes. Publishing Mining and Tunnel Construction. **21** (2), 30, **2015** [In Polish].
9. STRYCZEK S., GONET A., WIŚNIEWSKI R., ZŁOTKOWSKI A. The Influence of Selected Liquefiers on the Rheological Parameters of Cement Slurries. *AGH DRILLING, OIL, GAS*, **34** (3), **2017**.
10. CHUDEK M. Rock Mechanics with the Basics of Environmental Protection Management in Mining and Post-Mining Areas. Publishing House of the Silesian University of Technology, Gliwice **2010** [In Polish].
11. SCIGAŁA, R., SZAFULERA, K. Linear Discontinuous Deformations Created on the Surface as an Effect of Underground Mining and Local Geological Conditions - Case Study. *Bulletin of Engineering Geology and the Environment*, **79**, 2059, **2020**.
12. STRZAŁKOWSKI P., SZAFULERA K. Occurrence of Linear Discontinuous Deformations in Upper Silesia (Poland) in Conditions of Intensive Mining Extraction - Case Study. *Energies*, **13** (8), **2020**.

13. FAGIEWICZ K. Spatial Processes of Landscape Transformation in Mining Areas (Case Study of Opencast Lignite Mines in Morzysław, Niesłusz, Gosławice). *Polish Journal of Environmental Studies*, **23** (4), **2014**.
14. HUSSAIN J., ZHANG J., LINA X., HUSSAIN K., SHAH S.Y.A., ALI S., HUSSAIN A. Resource Assessment of Limestone Based on Engineering and Petrographic Analysis. *Civil Engineering Journal*, **8** (3), **2022**.
15. TALEBKEIKHAH M., SADEGHTABAGHI Z., SHABANI M. A Comparison of Machine Learning Approaches for Prediction of Permeability using Well Log Data in the Hydrocarbon Reservoirs. *Journal of Human, Earth and Future*, **2** (2), **2021**.
16. CHALIKAKIS K., PLAGNES V., GUERIN R., VALOIS R.I BOSH F.P. Contribution of Geophysical Methods to Karst System Exploration: an Overview. *Hydrogeological Journal*, **19**, 1169, **2011**.
17. VARNAVINA A., KHAMZIN A., KIDANU S., ANDERSON N. Geophysical Site Assessment in Karst Terrain: A Case Study From Southwestern Missouri. *Journal of Applied Geophysics*, **170**, November **2019**.
18. PISANO L., ZUMPARO V., PEPE M., LISO I.S., and PARISE M. Assessing Karst Landscape Degradation: A Case Study in Southern Italy. Published: MDPI - Land, **11**, **2022**.
19. RODZIK J., CIUPA T., JANICKI G., KOCIUBA W., TYC A., ZGŁOBICKI W. \Contemporary Transformations of the Relief of the Polish Highlands. Publishing House of the Institute of Geography and Spatial Management, Jagiellonian University, Kraków, **2008** [In Polish].
20. FADHLI Z., SAAD R., NORDIANA M., AZWIN N., BERY A. Mapping Subsurface Karst Formation Using 2D Electrical Resistivity Imaging (2DERI). *EJGE*, **20**, **2015**.
21. ISMAIL A., ANDERSON N. Pseudo-3D Electrical Resistivity Tomography Imaging of Subsurface Structure of a Sinkhole – A Case Study in Greene County, Missouri. *AIMS Geosciences*, **6**, 54, **2020**.
22. ARAFFA S., ATYA M., MOHAMED A., GABALA M., ZAHER M., SOLIMAN M., MESBAH H., MASSOUD U. I SHAABAN H. Subsurface Investigation on Quarter 27 of May 15th city, Cairo, Egypt Using Electrical Resistivity Tomography and Shallow Seismic Refraction Techniques. *NRIAG Journal of Astronomy and Geophysics*, **3** (2), 170, **2014**.
23. KOWALCZYK S., ŻUKOWSKA K.A., MENDECKI M. J., ŁUKASIAK D. Application of Electrical Resistivity Imaging (ERI) for the Assessment of Peat Properties: a Case Study of the Całowanie Fen, Central Poland. *Acta Geophysica*, **65** (1), 223, **2017**.
24. HUSSAIN Y., UAGODA R., BORGES W., NUNES J., HAMZA O., CONDORI C., ASLAM K., CÁRDENAS-SOTO M. The Potential Use of Geophysical Methods to Identify Cavities, Sinkholes and Pathways for Water Infiltration. *MDPI - Water* **12** (8), **2020**.
25. DÜZTAŞ E., KURTULUŞ B., ERDEM G., SAĞIR C., GÜRCAN T., AVŞAR Ö., REGNIER J., COZ M., RAZACK M. Electrical Resistivity Tomography (ERT) and Induced Polarization (IP) Applied to Karst Alluvium: Case Study from Azmak Spring, Mugla. *International Ground Water Conference, New Delhi, India*, **2017**.
26. GAO L., XIA J., PAN Y., XU Y. Reason and Condition for Mode Kissing in MASW Method. *Pure and Applied Geophysics*, **173** (5), 1627, **2016**.
27. ABDALLATIF T., KHOZYM A., GHANDOUR A. Determination of Seismic Site Class and Potential Geologic Hazards using Multi-Channel Analysis of Surface Waves(MASW) at the Industrial City of Abu Dhabi, UAE. *NRIAG JOURNAL OF ASTRONOMY AND GEOPHYSICS*, **11** (1), 193, **2022**.
28. CHOON P. ParkSEIS-3D for 3D MASW Surveys. *Fast Times*, **24** (4), 67, **2019**.
29. KORTAS Ł. Model Analysis of Microgravimetric Effects Recorded over Liquidated Mine Shafts. *Publishing Mining Review* **7**, 97, **2014** [In Polish].
30. NEAL A. Ground-Penetrating Radar and its Use in Sedimentology: Principles, Problems and Progress. *Earth-Science Reviews*, **6** (3-4), 261, **2004**.
31. MAHMOUDZADEH M.R., FRANCES A.P., LUBCZYNSKI M., LAMBOT S. Using Ground-Penetrating Radar to Investigate the Water Table depth in Weathered Granites – Sardon Case Study, Spain. *Journal of Applied Geophysics*, **79**, 17, **2012**.
32. LEUCCI G., SCARDOZZI G., DE GIORGI L., DITARANTO I., Miccoli I. Ground-Penetrating Radar and Electrical Resistivity Tomography Surveys at the Cerrate Abbey (Lecce, Italy). *Exploration Geophysics* **53** (5), 1, **2021**.